KeAi

CHINESE ROOTS
GLOBAL IMPACT

Contents lists available at ScienceDirect

# Petroleum Science

journal homepage: www.keaipublishing.com/en/journals/petroleum-science



Original Paper

# Non-Darcy flows in layered porous media (LPMs) with contrasting pore space structures



Xue-Yi Zhang, Zhi Dou\*, Jin-Guo Wang, Zhi-Fang Zhou, Chao Zhuang

School of Earth Sciences and Engineering, Hohai University, Nanjing 210098, Jiangsu, China

#### ARTICLE INFO

Article history: Received 18 October 2021 Received in revised form 13 April 2022 Accepted 27 May 2022 Available online 2 June 2022

Edited by Jie Hao

Keywords: Non-Darcy flow Layered porous media Heterogeneity Forchheimer equation Simulations

#### ABSTRACT

Compared to single layer porous media, fluid flow through layered porous media (LPMs) with contrasting pore space structures is more complex. This study constructed three-dimensional (3-D) pore-scale LPMs with different grain size ratios of 1.20, 1.47, and 1.76. The flow behavior in the constructed LPMs and single layer porous media was numerically investigated. A total of 178 numerical experimental data were collected in LPMs and single layer porous media. In all cases, two different flow regimes (i.e., Darcy and Non-Darcy) were observed. The influence of the interface of layers on Non-Darcy flow behavior in LPMs was analyzed based pore-scale flow data. It was found that the available correlations based on single layer porous media fail to predict the flow behavior in LPMs, especially for LPM with large grain size ratio. The effective permeability, which incorporated the influence of the interface is more accurate than the Kozeny-Carman equation for estimating the Darcy permeability of LPMs. The inertial pressure loss in LPMs, which determines the onset of the Non-Darcy flow, was underestimated when using a power law expression of mean grain size. The constant B, an empirical value in the classical Ergun equation, typically equals 1.75. The inertial pressure loss in LPMs can be significantly different from it in single lager porous media. For Non-Darcy flow in LPMs, it is necessary to consider a modified larger constant B to improve the accuracy of the Ergun empirical equation.

© 2022 The Authors. Publishing services by Elsevier B.V. on behalf of KeAi Communications Co. Ltd. This is an open access article under the CC BY license (http://creativecommons.org/licenses/by/4.0/).

# 1. Introduction

Layered porous medium (LPM) system, which refers to the porous medium that consisting of distinctly different pore space structures, grain sizes, and hydraulic properties in different layers or regions (Liang et al., 2019), is commonly encountered in the oil industry (Sharifi and Kelkar, 2013). The LPM tends to be heterogeneous on a macroscopic scale, e.g., structured soils (Martinez et al., 2021), fracture-matrix systems (Edery et al., 2016; Rostami et al., 2020), and aquifer-aquitard systems (Zhan et al., 2009). Characterizing accurately fluid flow behaviors within the LPM is of great importance for natural and industrial processes, such as groundwater flow in heterogeneous formations, solute transport in aquifer-aquitard systems (Berkowitz et al., 2009), and the process of miscible displacements (Afshari et al., 2018). Fluid flow across the interface of layers is a complex process. Previous studies (You and Liu, 2002; Chen et al., 2014; Landa-Marbán et al., 2019) had revealed that the interface between the free-flow and porous

medium systems can significantly affect the fluid flow and/or mass transfer. Goharzadeh et al. (2005) measured the interfacial velocity in free flow and porous medium systems and found that there is a drastic velocity gradient in the vertical direction between the pure fluid and the porous region. Such a vertical velocity gradient depends strongly on the Reynolds number and the porosity. Moreover, the complex velocity field can further control the interfacial mass-transfer dynamics (Kim and Kang, 2020).

Because of observational and computational limitations, it is still a challenge to directly measure fluid flow in the pore space. The interface of layers connects the pore space with different pore sizes. When a fluid flows across the interface, sudden contractions or expansions of the flow paths may occur, causing variations in flow velocity and directions. In recent decades, several studies (Vafai and Thiyagaraja, 1987; Berkowitz et al., 2009; Cortis and Zoia, 2009; Giacobbo et al., 2019) have attempted to accurately model the process of fluid flow across the interface of layers, which is considered essential for understanding the fundamental mechanics of fluid flow and mass transfer in formations or hydrological systems. With the development of computer performance, direct simulations, such as standard computational fluid dynamics (CFD)

E-mail address: Douz@hhu.edu.cn (Z. Dou).

<sup>\*</sup> Corresponding author.

(Anderson and Wendt, 1995) or Lattice Boltzmann Method (LBM) (Yu et al., 2003), and other methods (Yang et al., 2016), have been proposed and used in pore-scale research (Dou et al., 2013; Muljadi et al., 2016; El-Zehairy et al., 2019). Direct numerical simulation can provide information on the internal fluid flow of the porous media, which is beneficial for advancing our fundamental understanding of macro-scale flow phenomena (Dou et al., 2019; Wood et al., 2020).

Darcy's law (Darcy, 1856) is commonly used to depict fluid flow behavior in the porous medium. In the creeping flow regime, the relation between pressure p (Pa) and the seepage velocity U (m/s) is described by a linear Darcy equation:

$$\nabla p = \frac{\mu}{K_{\rm D}} \mathbf{U} = \frac{\mu}{K_{\rm D}} \frac{q}{A} \tag{1}$$

where  $\mu$  is the dynamic viscosity of fluid (Pa·s),  $K_D$  is the Darcy permeability ( $m^2$ ), **U** is the seepage velocity (m/s), q is the volume of fluid flow per unit time  $(m^3/s)$ , and A is the cross-sectional area of porous medium sliced perpendicular to the flow direction (m<sup>2</sup>). It has been well recognized; however, Darcy's law is only valid under a limited range of low velocity or Reynolds number (Re). As the velocity increase, fluid flow deviations from Darcy's law have long been observed. Non-Darcy flow occurs due to the non-negligible inertial losses caused by the variations in flow velocity or direction along the flow paths due to constrictions or obstructions (Fester et al., 2008; Chen et al., 2015; Yao et al., 2019). Understanding the fluid flow behaviors with high flow velocity in porous media is of great significance in many fields, such as groundwater hydrology, chemical, gas, and petroleum industries. To account for the inertial pressure loss, Forchheimer (1901) added a quadratic velocity term to represent the non-linear inertial effects:

$$\nabla p = \frac{\mu}{K_{\rm F}} \mathbf{U} + \beta \rho \mathbf{U}^2 \tag{2}$$

where  $K_{\rm F}$  is the Forchheimer permeability, and  $\beta$  is the non-Darcy coefficient or Forchheimer coefficient. Analysis of experimental data shows that deviation from Darcy's law is governed by the Forchheimer coefficient (Zolotukhin and Gayubov, 2021). In petroleum science, the Non-Darcy flow is common and significant for oil and gas exploration (Yao and Ge, 2011; Wang and Sheng, 2017; Kidogawa et al., 2021; Ma et al., 2022). Reservoir seepage characteristics are complex under high production rate conditions, especially in the near-wellbore region (Yao et al., 2015). Recently, more and more attention has been paid to the Non-Darcy flow in petroleum science (Saboorian-Jooybari and Pourafshary, 2015; Fan et al., 2019; Nie et al., 2021).

Previous studies of Non-Darcy flow deal only with the single layer porous media. Uniform spherical or cylindrical shapes of grains were used in a single layer, suggesting a relatively homogeneous pore space. Both laboratory experiments (van Lopik et al., 2017) and micromechanical simulations (Amiri et al., 2019) had shown that the grain sizes and pore space structures imposed remarkable effects on the onset of Non-Darcy or the transition of flow regimes in porous media. It was further found that the values of critical Reynolds number generally increase with the mean grain size. Li et al. (2019) investigated the Non-Darcy flow and the transition of flow regimes in a column with mixed grain sizes. Their results showed that for the mixtures of two grain sizes, the transition of flow regimes was affected by the mass ratio of these two grain sizes. However, they mixed the grains in a single layer. For a heterogeneous LPM system consisting of two distinct grains sizes, comprehensive studies on Non-Darcy flow and the transition of flow regimes are still limited.

The  $\beta$  is related to the inertial properties of the porous medium and plays a significant role in determining the inertial pressure loss. An appropriate  $\beta$  is essential for estimating Non-Darcy flow behavior. Many effects have been made to establish a link between the  $\beta$  and the properties of the porous medium, such as porosity, permeability, grain and pore size distribution (van Lopik et al., 2017), tortuosity, specific surface area, and surface roughness (Chen et al., 2015). Various relational formulas (Ergun, 1952: Geertsma, 1974; Kundu et al., 2016; Muljadi et al., 2016; Huang et al., 2020) have been proposed based on the experimental or numerical databases obtained in single layer porous media. However, the existing empirical models are divergent as the empirical models have been built based on different porous media types. It has been reported that the  $\beta$  obtained by field experiments tends to be two to three times higher than the value calculated by empirical models. Since the  $\beta$  is sensitive to the pore space structure, the influence of the sudden constriction of the pore space at the interface of layers on the pressure loss cannot be neglected. The higher complexity of pore space will magnify fluid inertial effects (Nissan and Berkowitz, 2018). To our best knowledge, the study focusing on the  $\beta$  in LPM is rarely reported. How the interface of layers affects the inertial pressure loss and Non-Darcy flow behavior is not yet known.

The purpose of this study is to accurately characterize Non-Darcy flow behavior in LPMs with contrasting pore space structures and to investigate the influence of the interface on Non-Darcy flow. Non-Darcy flow is common in LPMs but has not been fully investigated, which motivated this study. More specifically, we first constructed 3-D LPMs consisting of coarse and fine grain layers. There were three grain size ratios for coarse and fine grain layers, representing contrasting pore space structures. Numerical simulations of fluid flow were performed in the constructed LPMs at a range of pressure gradients. The influence of interface of layers on Darcy permeability, the onset of Non-Darcy flow, and the estimation of inertial pressure loss was evaluated based on the numerical results. The capability of previous correlations for predicting Non-Darcy flow behavior was discussed in this paper.

# 2. Methodology

#### 2.1. Numerical simulation set-up

Since intrapore observations are rare and challenging to collect, the laboratory experiment is limited in investigating the complex fluid flow process in the micropore pore space. Instead, numerical modeling has become an essential tool for studying the mechanism of fluid flow in porous media. Moreover, the pore-scale modeling can provide detailed information about the physical processes in the micropore space and the macroscale phenomenon. We contracted a 3-D pore-scale cylindrical LPM where consists of two contrasting layers (the coarse grain layer and the fine grain layer, see Fig. 1a) to investigate non-Darcy flow across the interface. In LPM, each layer was constructed based on deposition and collision processes under the force of gravity (Cundall and Strack, 1979; Pilotti, 1998). All spherical grains were filled into the tube, which had a length (L) of 60 mm and a diameter (D) of 12 mm. The spherical grains with two contrasting sizes were adopted to represent the coarse and fine grains in adjacent layers. Each layer was 30 mm long, half the length of the entire LPM. There was a sharp interface in the midplane, the junction between the coarse grain and fine grain layers.

In this study, three 3-D LPMs with different grains size ratios  $(\overline{d_c}/\overline{d_f})$  of 1.20, 1.47, and 1.76 were constructed. The spherical grains in each layer were set to follow the truncated lognormal

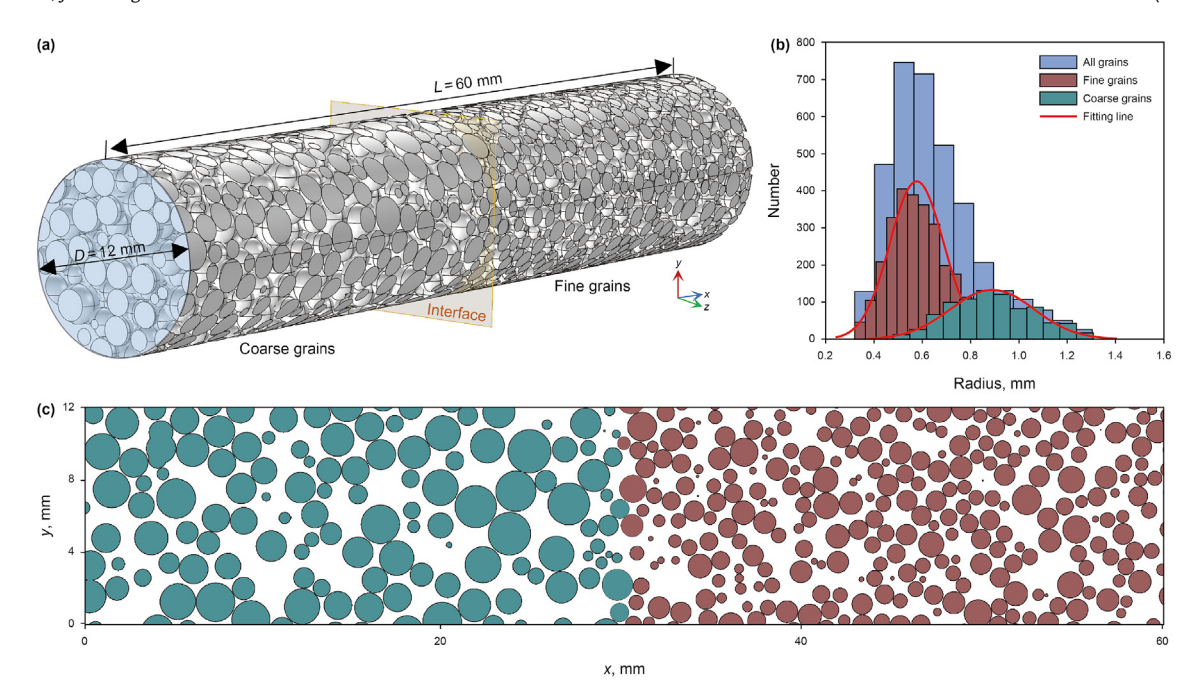


**Fig. 1.** (a) The 3-D LPM of Case 2  $(\overline{d_c}/\overline{d_f} = 1.47)$  consists of a coarse grain layer and a fine grain layer; (b) the grain size distribution of the coarse grains, fine grains, and all grains; the grain size follows the truncated lognormal distribution (red line); (c) the 2-D cross-section of the 3-D LPM.

distribution (Hochstetler et al., 2013), consistent with the feature of nature grain size distribution. Take case 2 as an example, the mean coarse grain size  $\overline{d_c}$  and the standard deviation  $\overline{\delta_c}$  of coarse grain size was set to 1.70 mm and 0.34 mm, respectively. The  $\overline{d_f}$  and  $\overline{\delta_f}$  for the fine grain size was set to 1.20 mm and 0.24 mm, respectively. Thus, the coefficient of grain size variation (COV =  $\delta/\overline{d}$ ) in each layer were kept at 0.2. The information of three LPMs and the corresponding coarse grain layer or fine grain layer were summarized in Table 1.

The grain size distribution in LPM was broader than the grain size distribution in the fine grain layer or coarse grain layer (see Fig. 1b). Due to grain size variation and random distribution of grain position, the pore space structure was highly heterogeneous. Meanwhile, as shown in the 2-D cross-section (see Fig. 1c), there were two distinct pore spaces in different layers. The pore space size in the coarse grain layer was relatively larger than that in the fine grain layers. A sudden contraction of pore space size occurred at the interface of layers.

**Table 1** Information of 3-D layered porous media with different grain size ratios.

Parameters	Case 1	Case 2	Case 3
Grain size ratio $\overline{d_{\rm c}}/\overline{d_{\rm f}}$ $(-)$	1.20	1.47	1.76
<b>Mean grain size</b> $\overline{d}$ (mm)	1.46	1.44	1.42
Mean coarse grain size $\overline{d_c}$ (mm)	1.59	1.71	1.87
Mean fine grain size $\overline{d_f}$ (mm)	1.33	1.16	1.06
Porosity $\Phi(-)$	0.46	0.45	0.44
Porosity of coarse grain layer $\Phi_{c}$ (—)	0.46	0.45	0.43
Porosity of fine grain layer $\Phi_{\mathrm{f}}$ $(-)$	0.46	0.45	0.44
Tortuosity $^{a} T(-)$	1.27	1.26	1.28

<sup>&</sup>lt;sup>a</sup> The tortuosity of LPMs can be obtained from the fluid velocity field ( $T=\overline{V}/\overline{Vx}$ ,  $\overline{V}$  is the average magnitude of intrinsic velocity over the entire volume and  $\overline{Vx}$  is the volumetric average of its component along the main flow direction).

## 2.2. Governing equations and verification of the numerical method

The steady-state velocity fields were mapped by solving the full Navier-Stokes equation (NSE) and the continuity equation. For an isothermal, incompressible, and Newtonian fluid, flow through the pore space in the porous medium is given by:

$$\rho \mathbf{u} \cdot \nabla \mathbf{u} = -\nabla p + \mu \nabla^2 \mathbf{u} \tag{3}$$

$$\nabla \cdot \boldsymbol{u} = 0 \tag{4}$$

where  $\rho$  (998.2 kg/m³ at 20 °C) is the density of fluid,  $\mu$  is the dynamic viscosity of fluid (Pa·s), p is the fluid pressure (Pa), u is the velocity vector [u, v, w] (m/s). For each case, constant pressure boundary conditions were applied at inlet and outlet boundaries to form a series of pressure gradients over LPM and drive the fluid flow through LPM in the x-direction (see Fig. 1a). All grain and tube surfaces were set as no-slip boundaries.

Fluid flow simulations were performed applying pressure to the inlet boundary to drive fluid flow through the 3-D LPMs. The numerical simulations were implemented via the finite element software COMSOL Multiphysics. The flow simulations were run on a workstation with 24 processors and 128 Gb of memory. To overcome the solver convergence issues which are typically encountered at high pressure gradient conditions, we simulated flow with progressively and incrementally increasing  $\nabla p$  while using a preceding lower flow result as an initial solution. The computational domain for the porous medium was discretized into 15 070 425 Lagrange-triangular elements. And the mesh independence analysis was performed to ensure numerical stability and accuracy. The result showed that the numerically derived flow was not sensitive to a further refinement of mesh size, indicating that the 15 070 425 elements are sufficient to provide stable and accurate numerical results. The GMRES iterative solver with the multigrid preconditioner was used to solve equations. The outer preconditioner iterations were performed using the V-cycle multigrid cycle. We set the overall convergence criteria at  $1.0 \times 10^{-4}$ .

X.-Y. Zhang, Z. Dou, J.-G. Wang et al. Petroleum Science 19 (2022) 2004–2013

gradient Fluid flows under pressure conditions (0.0166–1.6597 Pa/m) were simulated in a rectangular simple pipe section (60 mm in length and 12 mm in height) to validate the numerical simulation method. A series of inlet pressure (corresponding seepage velocity **U** equal to 0.0001 m/s, 0.00025 m/s, 0.0005 m/s, 0.00075 m/s, 0.001 m/s, 0.0025 m/s, 0.005 m/s, 0.0075 m/s, and 0.01 m/s) were applied at the left inlet boundary to drive fluid flow in the pipe. The magnitude velocity data at a crosssection were obtained and be compared with the mechanistic analytical solution of the Navier-Stokes equation Eqs. (3) and (4):  $V(z) = -\frac{h^2}{8\mu} \frac{dp}{dx} \left(1 - \frac{4z^2}{h^2}\right)$ , where h is the height of the pipe and z is the vertical position. As shown in Fig. 2b, V at the pipe surface is equal to zero due to the non-slip boundary condition, and the maximum appears at the center of the pipe. The simulation results V(z) at the cross-section all shows parabolic velocity profiles and agree well with the mechanistic analytical solutions, indicating the numerical method can provide an accurate flow field.

## 2.3. Reynolds number and forchheimer number

The Reynolds number is commonly used to predict the onset of non-Darcy flow and has developed several definitions (Zeng and Grigg, 2006). The most widely adopted Reynolds number (Re) is defined as the ratio of inertial forces to viscous forces:

$$Re = \frac{d\rho \mathbf{U}}{\mu} \tag{5}$$

Forchheimer number (*Fo*) is also recommended as the criterion for non-Darcy flow in a porous medium by some scholars because it has the advantage of clear definition, sound physical meaning, and wide applicability (Zeng and Grigg, 2006). It reflected the ratio of pressure gradient required to overcome inertial forces to that of viscous forces. The critical value for non-Darcy flow varies from 0.05 to 0.2 for *Fo*. The *Fo* is defined as the ratio of non-linear to liner pressure loss in Forchheimer's law

$$Fo = \frac{\beta \rho \mathbf{U}^2}{\frac{\mu}{K_F} \mathbf{U}} = \frac{K_F \beta \rho \mathbf{U}}{\mu} \tag{6}$$

The point reflecting the transition from the Darcy and non-Darcy flow regime can be determined when dimensionless permeability  $K^* = 0.99$ , which means that the pressure loss due to the viscous term becomes less than 99% of the total pressure loss. In this study, the  $K^*$  is considered as

$$K^* = \frac{K_{\text{app}}}{K_{\text{D}}} \tag{7}$$

The  $K_{\text{app}}$  is apparent permeability and defined as

$$\frac{1}{K_{\rm app}} = \frac{\nabla p}{\mu \mathbf{U}} = \frac{1}{K_{\rm F}} + \frac{\beta \mathbf{U}}{\mu} \tag{8}$$

## 3. Results and discussion

# 3.1. Pressure gradient-seepage velocity relationships

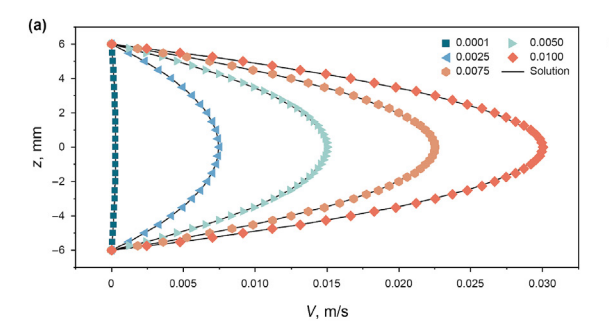
In this study, a series of numerical fluid flow simulations were performed in 3-D LPMs. The pressure gradient  $\nabla p$  between inlet and outlet boundaries varied from  $8.3 \times 10^{-3}$  to 108.3 kPa/m. resulting in a range of seepage velocities  $\boldsymbol{U}$  and different flow regimes. The flow fields in 3-D LPMs with different grain size ratios were shown in Fig. 3. A total of 178 numerical experimental data were collected in the form of  $\nabla p$  versus **U**. Fig. 4 is a plot of  $\nabla p$  versus **U** for all simulations in 3-D LPMs. It can be seen that the  $\nabla p$ increased nonlinearly with **U**, indicating that the flow regime varied from Darcy flow to Non-Darcy flow. When the **U** was somewhat the same, a finer grain size will lead to a larger  $\nabla p$ . This is because with finer grain size, the flow resistance becomes stronger and therefore a lager  $\nabla p$  is required to achieve the same *U*. Moreover, it was found that both Darcy flow and Non-Darcy flow in LPMs were different with the flow in single layer porous media. We investigated the influence of the interface on Darcy permeability, the onset of Non-Darcy flow, and the inertial pressure loss estimation when Non-Darcy occurs.

## 3.2. Darcy permeability

At low velocity (i.e., Re < 1 or Fo < 0.005), the inertial effects can be ignored, and the flow is Darcy regime. Based on the data where the Reynolds number was below the criterion for the onset of non-Darcy flow, the Darcy permeability ( $K_D$ ) for fine grain layer, coarse grain layer, and LPM were calculated for all cases and listed in Table 2. The onset of non-Darcy flow and its criteria will be discussed in section 3.3. As shown in Fig. 4b, d, f, for all cases, the relationship between pressure gradient  $\nabla p$  and seepage velocity  $\boldsymbol{U}$  matched Darcy's law (Eq. (1)) well ( $R^2 = 0.999$ ). The Kozeny-Carman equation can be used to predict the Darcy permeability of LPM:

$$K_{k-c} = \frac{\Phi^3}{kSv^2(1-\Phi)^2}$$
 (9)

where k is the Kozeny-Carman constant and Sv is the specific surface area. For the porous medium which consists of spherical grains,  $Sv = 6/\overline{d}$  and k = 5 for spherical grains (Kececioglu and Jiang,



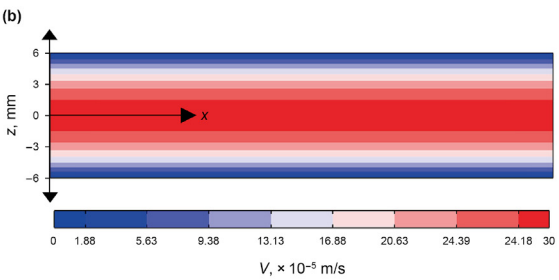


**Fig. 2.** Fluid flow in the simple pipe domain; (a) the simulation results V(z) at the cross-section for 5 selected seepage velocities compared with the mechanistic analytical solutions; (b) the magnitude velocity distribution in pipe takes the inlet seepage velocity 0.0001 m/s as an example.

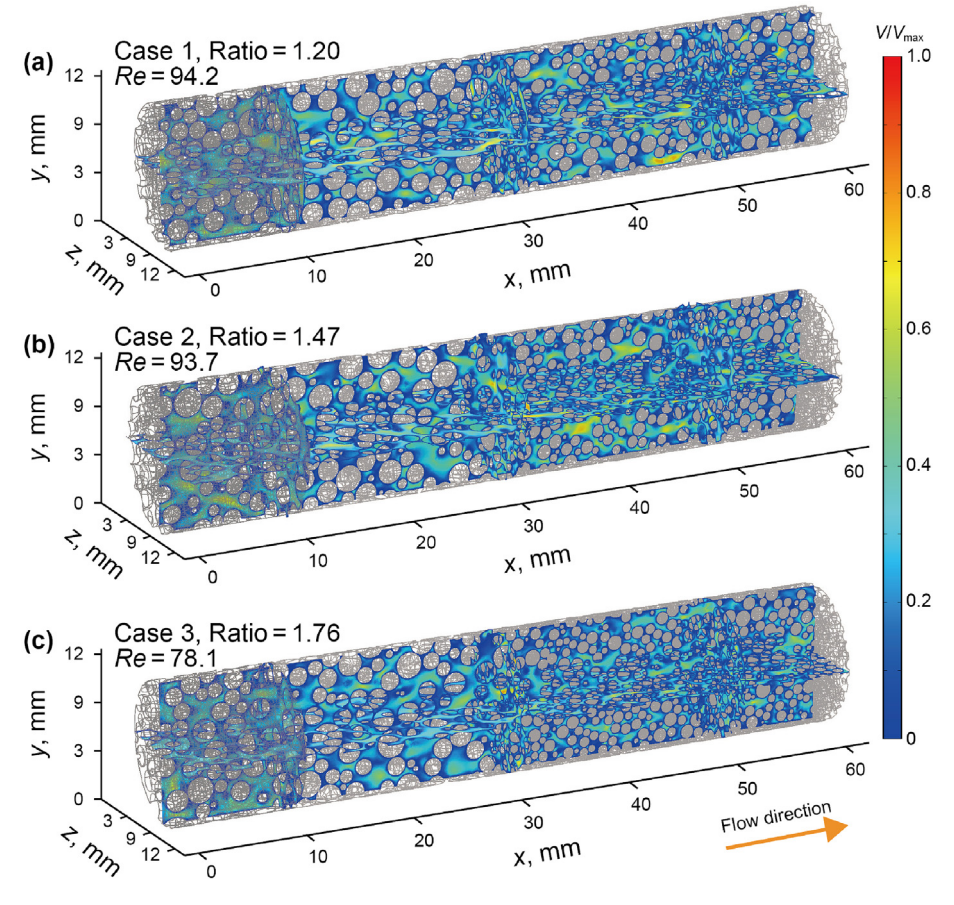


Fig. 3. Dimensionless magnitude of intrinsic velocity  $V/V_{max}$  in 3-D LPMs with contrasting pore space structures.

#### 1994)

As shown in Table 2, the Darcy permeability  $K_{\rm D}$  of LPM was between the  $K_{\rm D}$  of the coarse grain layer and the  $K_{\rm D}$  of the fine grain layer. The process of fluid flow through LPM was controlled by the two different pore space structures in the two layers. Since the Kozeny-Carman equation provides a robust prediction of permeability for porous media (i.e., sandy sediments) with relatively coarse grains (Ren and Santamarina, 2018). For the single layer porous medium, the results of  $K_{\rm K-C}$  were quite close to the  $K_{\rm D}$  obtained by simulations in all cases. However, for LPM, the  $K_{\rm K-C}$  predicted by the Kozeny-Carman equation gave a higher value than the  $K_{\rm D}$ . The relative errors between the  $K_{\rm K-C}$  and  $K_{\rm D}$  for LPM are larger than the errors for single layer porous medium. The accuracy of the Kozeny-Carman equation in predicting the Darcy permeability of LPM decreased compared with that in predicting the Darcy permeability of a single grain layer.

Therefore, it is necessary to consider the combined effects of layers and the interface on fluid flow through LPM. The effective permeability  $K_{\rm E}$  can be adopted to further homogenize the LPM and describe the combined effects on permeability. For LPM where the pressure at the interface is continuous, the effective permeability  $K_{\rm E}$  can be estimated as follows:

$$\frac{L_1 + L_2}{K_E} = \frac{L_1}{K_1} + \frac{L_2}{K_2} \tag{10}$$

where  $L_1$  and  $L_2$  are the lengths for the coarse grain layer and the fine grain layer,  $K_1$  and  $K_2$  are the permeability for each layer. In this study,  $L_1 = L_2$ ;  $K_1$  and  $K_2$  were equal to the  $K_{K-C}$  predicted by the Kozeny-Carman equation for the coarse grain layer and the fine

grain layer. As a result (see Table 2), the effective permeability  $K_{\rm E}$  could provide a much more accurate prediction of Darcy permeability than  $K_{\rm K-C}$ .

# 3.3. The onset of Non-Darcy flow

As shown in Fig. 4, at a point of divergence, the pressure gradient  $\nabla p$  begins to exhibit a non-linear relationship with seepage velocity  $\boldsymbol{U}$ , which is called the onset of the non-Darcy flow. Then the flow is gradually affected by inertial effects, leading to a decrease in permeability and the transition between Darcy and non-Darcy flow regimes. To investigate how the interface of layers affects the discrepancy between the non-Darcy flow and the Darcy flow, the flow fields within the pore space under several pressure gradients or Reynolds numbers were plotted. As depicted in Fig. 5, the eddies formed and grew near the interface as the pressure gradient increased. The size and structure of eddies depended strongly on the pressure gradients or Reynolds number and further influenced the flow fields. The streamlines were smoother in low pressure gradient cases than in high pressure gradient cases.

Moreover, the streamlines away from the interface were smoother than those near the interface. Since the eddies were more likely to develop near the interface where the pore space abruptly changes. The eddies could increase drag and decrease the permeability of the LPM, which causes the deviation from Darcy's law. This can be attributed to the fact that the developing eddies can decrease the effective flow paths (Chaudhary et al., 2011; Lee et al., 2014). It should be mentioned that the flow regime cannot be determined whether it is non-Darcy (non-linear flow) or Darcy

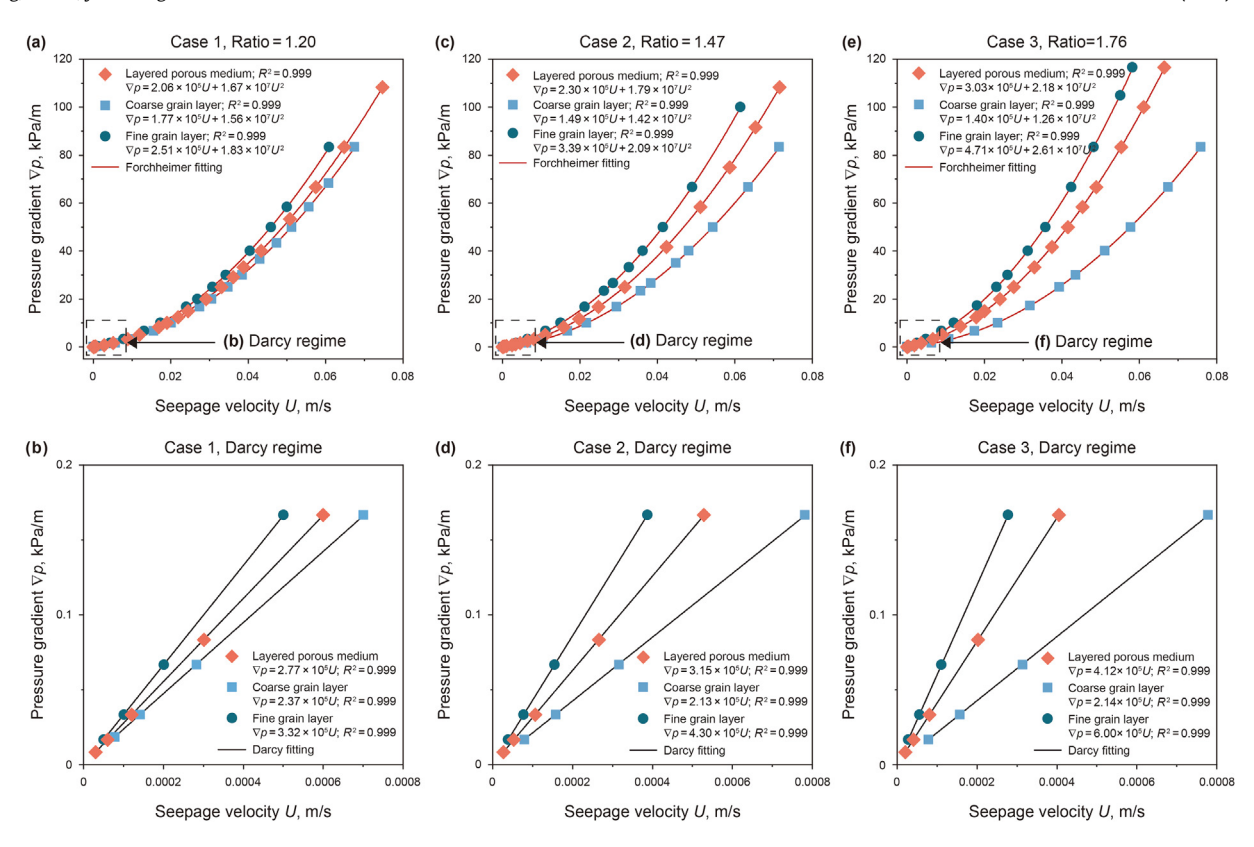


**Fig. 4.** Pressure gradient  $\nabla p$  as a function of seepage velocity U for coarse grain layers, fine grain layers, and LPMs obtained by numerical simulations (a, c, and e), for the conditions where the Reynolds number was below the criterion for the onset of non-Darcy flow (b, d, and f).

**Table 2** The results of Darcy permeability  $(K_D)$  were obtained from simulations, predicted by the Kozeny-Carman equation  $(K_{K-C})$ , and effective permeability equation  $(K_E)$ .

Cases	Samples	$K_{\rm D}( imes10^{-9}{ m m}^2)$	$K_{\text{K-C}}  (  imes  10^{-9}  \text{m}^2)$	$K_{\rm E}$ ( $ imes$ $10^{-9}$ ${ m m}^2$ )
Case 1	LPM	3.61	3.78	3.68
Ratio=1.20	Coarse grain layer	4.22	4.48	N/A
	Fine grain layer	3.01	3.13	N/A
Case 2	LPM	3.18	3.50	3.18
Ratio=1.47	Coarse grain layer	4.71	4.77	N/A
	Fine grain layer	2.33	2.39	N/A
Case 3	LPM	2.43	2.88	2.46
Ratio=1.76	Coarse grain layer	4.69	4.82	N/A
	Fine grain layer	1.67	1.65	N/A

(linear flow) based on the presence of eddies.

The onset of Non-Darcy flow can be determined when *K*\* equals 0.99. The critical Re and Fo, which indicate the cessation of the Darcy regime were summarized in Table 3. It can be seen that both the critical Re and Fo for the coarse grain layer were normally higher than those for LPM or fine grain layer. At the same time, the critical value for LPM was closer to the value for the fine grain layer than for the coarse grain layer, especially for the case with a large grain size ratio. This means that the onset of Non-Darcy flow in LPM depends more on the flow field in the fine grain layer. In the fine grain layer, which contained many more grains in the same volume, the grains had significantly increased the tortuous pore space structures. Meanwhile, in the LPM, fine grains caused the system to become less conductive. Thus, it will lead to a lower  $\boldsymbol{U}$  than in coarse grain layer under a certain pressure gradient, resulting in a smaller critical Re. In general, it is found that the onset of non-Darcy flow occurs earlier, at lower velocities, when the porous medium has a higher degree of heterogeneity and a lower permeability (El-Zehairy et al., 2019).

The coefficient of velocity variation (*CV*) also indicated that the fine grain layer and LPM exhibit a relatively higher degree of heterogeneity than coarse grain layer (see Table 3). The coefficient *CV*, a globe measure of the velocity spatial variability, can be used to quantitatively evaluate the heterogeneity of porous medium(Rolle and Kitanidis, 2014). For incompressible flow, *CV* is defined as follows:

$$CV = \frac{\sigma_{\boldsymbol{V}}}{\overline{\boldsymbol{V}}} = \frac{\sqrt{\int_{\Omega} (\boldsymbol{V} - \overline{\boldsymbol{V}})^2 \frac{d\Omega}{\Omega}}}{\int_{\Omega} \overline{\boldsymbol{V}} \frac{d\Omega}{\Omega}}$$
(11)

where the  $\sigma_{\pmb{V}}$  is the standard variance of the flow velocity,  $\overline{\pmb{V}}$  is the average magnitude of intrinsic velocity over the entire volume (the true velocity of fluid in the pores), and  $\Omega$  is the volume of the pore space occupied by fluid.

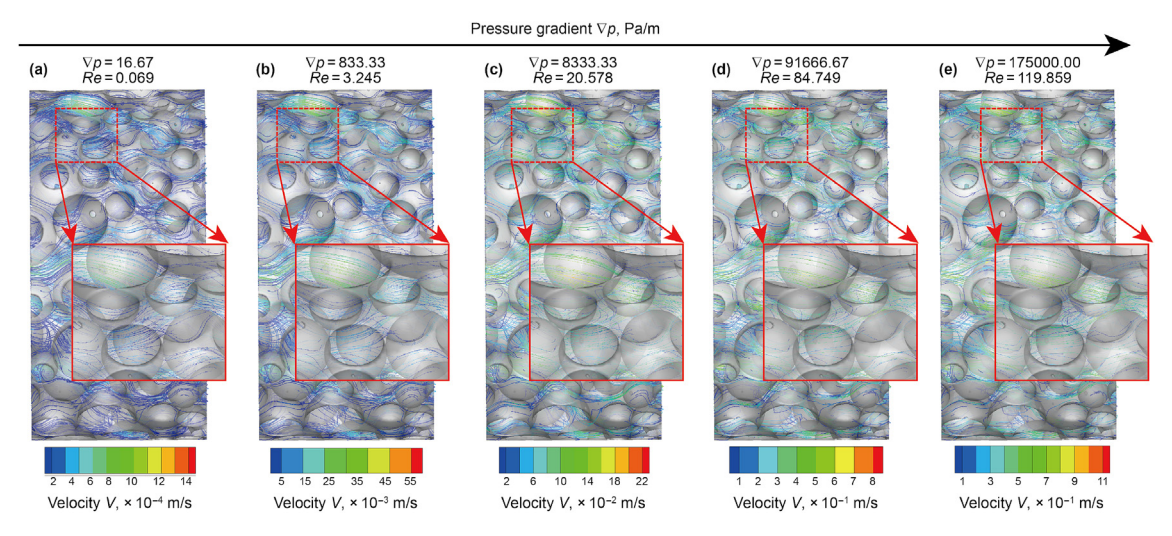


Fig. 5. Streamlines in LPM of case 2 for five pressure gradients; fluid flows across the interface between the coarse grains layer and the fine grains layer, and the flow regime varies from the Darcy regime to the non-Darcy regime.

**Table 3**Criteria (i.e., *Re* and *Fo*) for the onset of non-Darcy flow in LPMs and the corresponding coarse and fine grain layers; the coefficient of velocity variation (*CV*) for LPMs and single layer porous media.

Cases	Samples	Re	Fo	CV
Case 1	LPM	1.291	0.072	1.00
Ratio=1.20	Coarse grain layer	1.535	0.085	1.01
	Fine grain layer	1.268	0.070	1.01
Case 2	LPM	1.364	0.074	1.00
Ratio=1.47	Coarse grain layer	1.734	0.097	1.00
	Fine grain layer	1.040	0.055	1.02
Case 3	LPM	1.120	0.057	1.02
Ratio=1.76	Coarse grain layer	1.969	0.099	0.97
	Fine grain layer	0.947	0.037	1.01

# 3.4. Inertial pressure loss estimation

According to the non-linear Forchheimer Equation (Eq. (2)), the Forchheimer coefficient ( $\beta$ ) is ated to the inertial pressure loss in Non-Darcy flow. An appropriate  $\beta$  is essential for estimating the degree of flow nonlinearity and the transition between Darcy and Non-Darcy flow. The  $\beta$  calculated by empirical models usually exists in significant variations since the models of  $\beta$  were established based on various porous medium types (see Table 4). In this study,  $\beta$  was determined by fitting the plot of the pressure gradient  $\nabla p$ 

versus seepage velocity **U** using Eq. (2). As shown in Fig. 4, good agreement between the fits was found for all the samples studied  $(R^2 = 0.999)$ . The results of  $\beta$  were 16694, 17948, and 21827, respectively, for case1-3. However, the empirical models obtained from single layer porous media are not able to predict the  $\beta$  of LPMs. The model proposed by Geertsma (1974) gave the best prediction. However, it still underestimated the  $\beta$  of LPMs and gave the value of 6279, 7064, and 10545. Given that the  $\beta$  reflects the intrinsic properties of the porous medium, similar to the permeability  $K_D$ . For porous medium, previous empirical models to predict  $\beta$  have shown a power law relationship between  $\beta$  and  $K_D$ . By the Kozeny-Carman equation (Eq. (9)) and the fact that  $\beta$  decreases with the grain size growth, Forchheimer coefficient  $\beta$  can be estimated as a function of grain size  $\overline{d}$ . As shown in Fig. 6, a power law expression  $\beta = a\overline{d}^{-m}$  (a and m are regression coefficients) may be adequately used to predict  $\beta$  for a single layer porous medium.

As shown in Fig. 6, although the mean grain sizes for three LPMs are pretty close, there are still huge discrepancies between the three cases. Meanwhile, the  $\beta$  in LPMs deviates from the prediction curve obtained by the single layer porous medium. The relative error increases with the grain size ratio. The deviations can be attributed to the sudden pore space constriction between coarse and fine grain layers at the interface. As the grain size ratio increases, the discrepancies of the pore space in coarse and fine grain

**Table 4** Literature summary of available empirical models for estimate Forchheimer coefficient  $\beta$ 

Reference	Empirical model $eta$	Units of $\beta$ and $K_{\mathrm{D}}$	Media type
Janicek and Katz (1955)	$\frac{1.82E8}{K_{\rm D}^{1.25}\Phi^{0.75}}$	m <sup>-1</sup> , mD	Sandstone, limestone, dolomite
Geertsma (1974)	$\frac{6.005}{K_{D}^{0.5}\Phi^{5.5}}$	$cm^{-1}$ , $cm^2$	Unconsolidated/consolidated sandstones
Pascal and Quillian (1980)	$\frac{4.8E12}{K_{\rm D}^{1.176}}$	$\mathrm{m}^{-1},\mathrm{mD}$	Fracture
Cheng et al. (2019) <sup>a</sup>	$\frac{2.7E8(1-\Phi)}{\Phi^3} \left(\frac{S}{K_{\rm D}}\right)^{1/3}$	$\mathrm{m}^{-1}$ , $\mathrm{mD}$	Numerical porous media
Zhang et al. (2013)	$\frac{\omega(1-\Phi)}{K_{\rm D}\Phi^3}$	$m^{-1}$ , $m$	Concrete-sphere and crushed-rock layer
Zolotukhin and Gayubov (2021)	$\left(\frac{\Phi l^2}{K_{\rm D}}\right)^{0.47} \frac{(9.67E - 5)}{K_{\rm D}^{0.5} \Phi^{1.5}}$	m <sup>-1</sup> , m	Various porous media

 $<sup>^{\</sup>mathrm{a}}$  S denotes the specific surface area;  $\omega$  is the characteristic coefficient of particles.

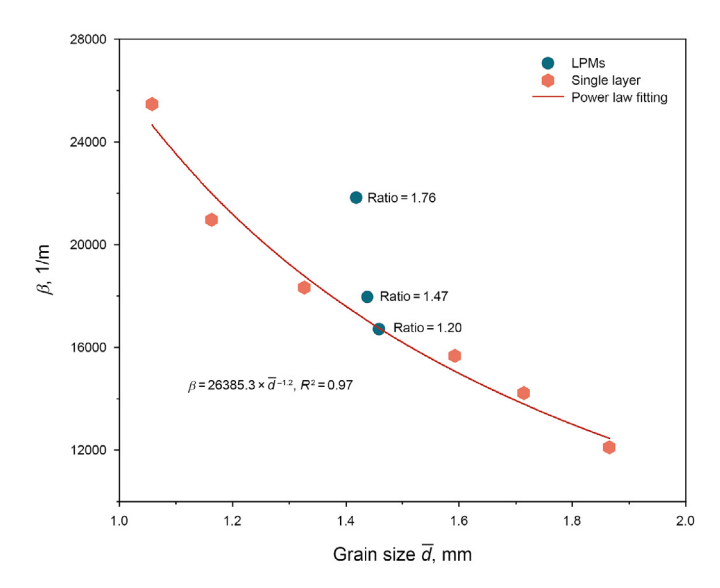


**Fig. 6.** A power-law relationship between Forchheimer coefficient  $\beta$  and grains size for a single layer.

layers become stronger. The sudden pore space constriction led to flow velocity or direction fluctuations and finally caused additional inertial losses. Therefore, for the LPMs, only considering the mean grains size may underestimate the pressure loss when Non-Darcy flow occurs.

The sensitivity analysis results indicate that the porosity significantly impacts the pressure loss in porous medium and makes estimating fluid flow behavior more complicated (Amiri et al., 2019). The pressure gradient across the packed porous medium is also generally estimated using the semi-empirical Ergun empirical equation. Ergun (1952) proposed an empirical model by analyzing the data from 640 experiments to approximate the  $\beta$ . There was various media in his experiments, which included spheres, sand, and pulverized coke. Ergun (1952)'s  $\beta$  is formulated as:

$$\beta_{\text{Ergun}} = \frac{B^*(1-\Phi)}{\overline{d}^*\Phi^3} \tag{12}$$

where B is a constant and equal to 1.75 by Ergun (1952). However, B is widely debated as it may vary with porous media and fluid velocity. Du Plessis and Woudberg (2008) suggested constant B equal 1.35 to 2.00 at porosities ranging from 0.20 to 0.80. A relatively larger constant B ranges from 12.1 to 14.1 have also been reported for some cases (Kyan et al., 1970). To our knowledge, the original or modified constants B are usually proposed based on the experimental results on the single layer porous media. It is necessary to use a modified constant B specific to LPMs to improve the accuracy in predicting the non-Darcy flow in LPM.

From the Eq. (12) and the  $\beta$  (see Fig. 6) for LPM, the constant B

**Table 5** Forchheimer coefficient  $\beta$  and the constant B in Ergun empirical equation for LPM, coarse grain layer, and fine grain layer in three cases with different grain size ratios.

Parameters	Samples	Case 1	Case 2	Case 3
Forchheimer coefficient $\beta$	LPM	16694	17948	21827
	Coarse grain layer	15661	14225	12621
	Fine grain layer	18337	20975	26141
Constant B	LPM	5.22	5.54	4.51
	Coarse grain layer	4.32	3.94	3.34
	Fine grain layer	4.24	4.22	4.12

for LPM can be calculated. According to the results (see Table 5) in this study, the constant B is generally larger for LPM than for single layer porous medium. Our result for the constant B is also larger than the empirical value proposed before. This can be attributed to our cases having a slightly larger porosity than the porosity in previous experiments. But the results may still reveal some problems. Therefore, to avoid misestimating the inertial pressure loss, a larger constant B is suggested for LPM when using the Ergun empirical equation to predict the pressure loss in the Non-Darcy flow regime.

## 4. Summary and conclusion

Compared to the single grain layer with a relatively homogeneous pore space structure, there were two distinct contrasting pore space structures in LPM. At the interface of the layers, there was a sudden contraction of the pore space, which could vary the flow velocity and direction. In this study, 3-D pore scale LPMs with different grain size ratios and 3-D pore scale single layer porous media were constructed to investigate the influence of the interface on the Non-Darcy flow. The Galerkin finite-element method was used to solve the full Native-Stokes equation directly. A total of 178 numerical experimental data and pore-scale flow fields were collected in LPMs and single layer porous media. In all cases, both the Darcy flow regime and the Non-Darcy flow regime were captured and discussed. The results showed that the interface between the layers significantly affects the fluid flow and the transition of the flow regime in LPMs.

By comparing the Darcy permeability in single layer porous media and LPMs, it was found that the Kozeny-Carman equation could predict the calculated  $K_{\rm D}$  of single layer porous media accurately. But the Kozeny-Carman equation failed to predict the calculated  $K_{\rm D}$  of LPMs and the deviation between prediction and estimated  $K_{\rm D}$  increased with the grain size ratio. It is essential to consider the interface of layers, especially for the case with highly contrasting pore space structures. The onset of Non-Darcy in three LPMs was estimated based on the dimensionless permeability  $K^*$ . The critical Reynolds number and Forchheimer number for Non-Darcy flow in LPMs were first discussed in this paper. The results showed that the critical Re for LPMs were similar to that for single layer porous media and was about 1.0. Moreover, it was found that the onset of Non-Darcy in LPM was more dependent on the fine grain layer.

Forchheimer coefficients  $\beta$  which relates to the inertial pressure loss in Non-Darcy flow were calculated for all cases. The  $\beta$  for single layer porous media can be estimated by a power law expression versus mean grain size. It was found that, however, the trend for  $\beta$  of LPMs deviated from the tendency for  $\beta$  of single layer porous media, especially for the case with a larger grain ratio. For the LPMs, considering the mean grains size alone may underestimate the pressure loss when Non-Darcy flow occurs. The constant B in Ergun empirical equation was first calculated for LPM. A larger constant B for LPMs than for single layer porous media was suggested for estimating the inertial pressure loss.

#### **Conflicts of interest**

The authors declare that they have no known competing financial interests or personal relationships that could have appeared to influence the work reported in this paper.

## Acknowledgment

The study is financially supported by the National Key Research and Development Program of China (No. 2019YFC1804303) and the

National Natural Science Foundation of China (Grant Nos. 41877171 and 41831289). The authors thank the editors and anonymous reviewers for their suggestions in improving the manuscript.

#### References

- Afshari, S., Hejazi, S.H., Kantzas, A., 2018. Longitudinal dispersion in heterogeneous layered porous media during stable and unstable pore-scale miscible displacements. Adv. Water Resour. 119, 125–141. https://doi.org/10.1016/ i.advwatres.2018.06.005.
- Amiri, L., Ghoreishi-Madiseh, S.A., Hassani, F.P., et al., 2019. Estimating pressure drop and Ergun/Forchheimer parameters of flow through packed bed of spheres with large particle diameters. Powder Technol. 356, 310–324. https://doi.org/10.1016/j.powtec.2019.08.029.
- Anderson, J.D., Wendt, J., 1995. Computational Fluid Dynamics. Springer, New York, pp. 3–14.
- Berkowitz, B., Cortis, A., Dror, I., et al., 2009. Laboratory experiments on dispersive transport across interfaces: the role of flow direction. Water Resour. Res. 45 (2). https://doi.org/10.1029/2008wr007342.
- Chaudhary, K., Cardenas, M.B., Deng, W., et al., 2011. The role of eddies inside pores in the transition from Darcy to Forchheimer flows. Geophys. Res. Lett. 38 (24). https://doi.org/10.1029/2011gl050214 n/a-n/a.
- Chen, J., Sun, S.Y., Wang, X.P., 2014. A numerical method for a model of two-phase flow in a coupled free flow and porous media system. J. Comput. Phys. 268, 1–16. https://doi.org/10.1016/j.jcp.2014.02.043.
- Chen, Y.F., Zhou, J.Q., Hu, S.H., et al., 2015. Evaluation of Forchheimer equation coefficients for non-Darcy flow in deformable rough-walled fractures. J. Hydrol. 529, 993–1006. https://doi.org/10.1016/j.jhydrol.2015.09.021.
- Cheng, Z.L., Ning, Z.F., Wang, Q., et al., 2019. The effect of pore structure on non-Darcy flow in porous media using the lattice Boltzmann method. J. Petrol. Sci. Eng. 172, 391–400. https://doi.org/10.1016/j.petrol.2018.09.066.
- Cortis, A., Zoia, A., 2009. Model of dispersive transport across sharp interfaces between porous materials. Phys. Rev. 80 (1), 011122. https://doi.org/10.1103/PhysRevE.80.011122.
- Cundall, P.A., Strack, O.D.L., 1979. A discrete numerical model for granular assemblies. Geotechnique 29 (1), 47–65. https://doi.org/10.1680/geot.1979.29.1.47.
- Darcy, H., 1856. Les fontaines publiques de la ville de Dijon: exposition et application. Victor Dalmont, Paris, pp. 1–8.
- Dou, Z., Zhang, X.Y., Chen, Z., et al., 2019. Effects of cemented porous media on temporal mixing behavior of conservative solute transport. Water 11 (6), 1204. https://doi.org/10.3390/w11061204.
- Dou, Z., Zhou, Z.F., Sleep, B.E., 2013. Influence of wettability on interfacial area during immiscible liquid invasion into a 3D self-affine rough fracture: lattice Boltzmann simulations. Adv. Water Resour. 61, 1–11. https://doi.org/10.1016/ j.advwatres.2013.08.007.
- Du Plessis, J.P., Woudberg, S., 2008. Pore-scale derivation of the Ergun equation to enhance its adaptability and generalization. Chem. Eng. Sci. 63 (9), 2576–2586. https://doi.org/10.1016/j.ces.2008.02.017.
- Edery, Y., Geiger, S., Berkowitz, B., 2016. Structural controls on anomalous transport in fractured porous rock. Water Resour. Res. 52 (7), 5634–5643. https://doi.org/ 10.1002/2016wr018942.
- El-Zehairy, A.A., Nezhad, M.M., Joekar-Niasar, V., et al., 2019. Pore-network modelling of non-Darcy flow through heterogeneous porous media. Adv. Water Resour. 131, 103378. https://doi.org/10.1016/j.advwatres.2019.103378.
- Ergun, S., 1952. Fluid flow through packed columns. Chem. Eng. Prog. 48, 89–94.
- Fan, M., McClure, J., Han, Y.H., et al., 2019. Using an experiment/simulation-integrated approach to investigate fracture-conductivity evolution and non-Darcy flow in a proppant-supported hydraulic fracture. SPE J. 24 (4), 1912–1928. https://doi.org/10.2118/195588-pa.
- Fester, V., Mbiya, B., Slatter, P., 2008. Energy losses of non-Newtonian fluids in sudden pipe contractions. Chem. Eng. J. 145 (1), 57–63. https://doi.org/10.1016/j.cej.2008.03.003.
- Forchheimer, P., 1901. Wasserbewegung durch boden. Z Ver Deutsch, Ing. 45, 1782–1788.
- Geertsma, J., 1974. Estimating the coefficient of inertial resistance in fluid flow through porous media. Soc. Petrol. Eng. J. 14 (5), 445–450. https://doi.org/10.2118/4706-pa.
- Giacobbo, F., Giudici, M., Da Ros, M., 2019. About the dependence of breakthrough curves on flow direction in column experiments of transport across a sharp interface separating different porous materials. Geofluids 2019, 1–8. https://doi.org/10.1155/2019/8348175.
- Goharzadeh, A., Khalili, A., Jørgensen, B.B., 2005. Transition layer thickness at a fluid-porous interface. Phys. Fluids 17 (5), 057102. https://doi.org/10.1063/
- Hochstetler, D.L., Rolle, M., Chiogna, G., et al., 2013. Effects of compound-specific transverse mixing on steady-state reactive plumes: insights from pore-scale simulations and Darcy-scale experiments. Adv. Water Resour. 54, 1–10. https://doi.org/10.1016/j.advwatres.2012.12.007.
- Huang, T., Du, P.B., Peng, X.K., et al., 2020. Pressure drop and fractal non-Darcy coefficient model for fluid flow through porous media. J. Petrol. Sci. Eng. 184. https://doi.org/10.1016/j.petrol.2019.106579.
- Janicek, J.D., Katz, D.L.V., 1955. Applications of unsteady state gas flow calculations. In: Proceed-ings of University of Michigan Research Conference.

- Kececioglu, I., Jiang, Y., 1994. Flow through porous media of packed spheres saturated with water. J. Fluid Eng. 116 (1), 164–170. https://doi.org/10.1115/12910229
- Kidogawa, R., Yoshida, N., Fuse, K., et al., 2021. Productivity improvement by reperforation of multistage-fractured wells in high-pressure/high-temperature tight gas reservoirs: a case history. SPE Prod. Oper. 36 (1), 97–115. https:// doi.org/10.2118/197590-pa.
- Kim, J.S., Kang, P.K., 2020. Anomalous transport through free-flow-porous media interface: pore-scale simulation and predictive modeling. Adv. Water Resour. 135, 103467. https://doi.org/10.1016/j.advwatres.2019.103467.
- Kundu, P., Kumar, V., Mishra, I.M., 2016. Experimental and numerical investigation of fluid flow hydrodynamics in porous media: characterization of pre-Darcy, Darcy and non-Darcy flow regimes. Powder Technol. 303, 278–291. https:// doi.org/10.1016/j.powtec.2016.09.037.
- Kyan, C.P., Wasan, D.T., Kintner, R.C., 1970. Flow of single-phase fluids through fibrous beds. Ind. Eng. Chem. Fundam. 9 (4), 596–603. https://doi.org/10.1021/i160036a012
- Landa-Marbán, D., Liu, N., Pop, I.S., et al., 2019. A pore-scale model for permeable biofilm: numerical simulations and laboratory experiments. Transport Porous Media 127 (3), 643–660. https://doi.org/10.1007/s11242-018-1218-8.
- Lee, S.H., Lee, K.-K., Yeo, I.W., 2014. Assessment of the validity of Stokes and Reynolds equations for fluid flow through a rough-walled fracture with flow imaging. Geophys. Res. Lett. 41 (13), 4578–4585. https://doi.org/10.1002/2014c1060481
- Li, Z.X., Wan, J.W., Zhan, H.B., et al., 2019. Particle size distribution on Forchheimer flow and transition of flow regimes in porous media. J. Hydrol. 574, 1–11. https://doi.org/10.1016/j.jhydrol.2019.04.026.
- Liang, X.Y., Zhang, Y.K., Liu, J., et al., 2019. Solute transport with linear reactions in porous media with layered structure: a semi-analytical model. Water Resour. Res. 55 (6), 5102–5118. https://doi.org/10.1029/2019wr024778.
- Ma, S., Ju, B.S., Zhao, L., et al., 2022. Embedded discrete fracture modeling: flow diagnostics, non-Darcy flow, and well placement optimization. J. Petrol. Sci. Eng. 208, 109477. https://doi.org/10.1016/j.petrol.2021.109477.
- Martinez, P., Buurman, P., do Nascimento, D.L., et al., 2021. Substantial changes in podzol morphology after tree-roots modify soil porosity and hydrology in a tropical coastal rainforest. Plant Soil 463, 77–95. https://doi.org/10.1007/s11104-021-04896-y.
- Muljadi, B.P., Blunt, M.J., Raeini, A.Q., et al., 2016. The impact of porous media heterogeneity on non-Darcy flow behaviour from pore-scale simulation. Adv. Water Resour. 95, 329–340. https://doi.org/10.1016/j.advwatres.2015.05.019.
- Nie, R.-S., Fan, X., Li, M., et al., 2021. Physical simulation of the nonlinear transient flow behavior in closed high-pressure gas reservoirs. Part I: pressure-depleted flow experiments on matrix cores. J. Petrol. Sci. Eng. 196, 108063. https:// doi.org/10.1016/j.petrol.2020.108063.
- Nissan, A., Berkowitz, B., 2018. Inertial effects on flow and transport in heterogeneous porous media. Phys. Rev. Lett. 120 (5), 054504. https://doi.org/10.1103/PhysRevLett.120.054504.
- Pascal, H., Quillian, R.G., 1980. Analysis of vertical fracture length And non-Darcy flow coefficient using variable rate tests. In: Proceedings of SPE Annual Technical Conference and Exhibition. https://doi.org/10.2118/9348-MS. SPE-9348-MS.
- Pilotti, M., 1998. Generation of realistic porous media by grains sedimentation. Transport Porous Media 33 (3), 257–278. https://doi.org/10.1023/A: 1006598029153.
- Ren, X.W., Santamarina, J.C., 2018. The hydraulic conductivity of sediments: a pore size perspective. Eng. Geol. 233, 48–54. https://doi.org/10.1016/j.enggeo.2017.11.022.
- Rolle, M., Kitanidis, P.K., 2014. Effects of compound-specific dilution on transient transport and solute breakthrough: a pore-scale analysis. Adv. Water Resour. 71, 186–199. https://doi.org/10.1016/j.advwatres.2014.06.012.
- Rostami, P., Sharifi, M., Dejam, M., 2020. Shape factor for regular and irregular matrix blocks in fractured porous media. Petrol. Sci. 17 (1), 136–152. https:// doi.org/10.1007/s12182-019-00399-9.
- Saboorian-Jooybari, H., Pourafshary, P., 2015. Significance of non-Darcy flow effect in fractured tight reservoirs. J. Nat. Gas Sci. Eng. 24, 132–143. https://doi.org/ 10.1016/j.jngse.2015.03.003.
- Sharifi, M., Kelkar, M., 2013. New dynamic permeability upscaling method for flow simulation under depletion drive and no-crossflow conditions. Petrol. Sci. 10 (2), 233–241. https://doi.org/10.1007/s12182-013-0272-7.
- Vafai, K., Thiyagaraja, R., 1987. Analysis of flow and heat transfer at the interface region of a porous medium. Int. J. Heat Mass Tran. 30 (7), 1391–1405. https://doi.org/10.1016/0017-9310(87)90171-2.
- van Lopik, J.H., Snoeijers, R., van Dooren, T.C.G.W., et al., 2017. The effect of grain size distribution on nonlinear flow behavior in sandy porous media. Transport Porous Media 120 (1), 37–66. https://doi.org/10.1007/s11242-017-0903-3.
- Wang, X.K., Sheng, J., 2017. Gas sorption and non-Darcy flow in shale reservoirs. Petrol. Sci. 14 (4), 746–754. https://doi.org/10.1007/s12182-017-0180-3.
- Wood, B.D., He, X., Apte, S.V., 2020. Modeling turbulent flows in porous media. Annu. Rev. Fluid Mech. 52 (1), 171–203. https://doi.org/10.1146/annurev-fluid-010719-060317.
- Yang, X.F., Mehmani, Y., Perkins, W.A., et al., 2016. Intercomparison of 3D pore-scale flow and solute transport simulation methods. Adv. Water Resour. 95, 176—189. https://doi.org/10.1016/j.advwatres.2015.09.015.
- Yao, L.M., Liu, J.B., Li, X.Y., et al., 2019. Application of the building block approach to characterize the pressure loss of water and fracturing fluid in contraction-

- expansion pipe. J. Petrol. Sci. Eng. 176, 51–61. https://doi.org/10.1016/i.petrol.2018.12.010
- Yao, Y.D., Ge, J.L., 2011. Characteristics of non-Darcy flow in low-permeability reservoirs. Petrol. Sci. 8 (1), 55–62. https://doi.org/10.1007/s12182-011-0115-3.
- Yao, Y.D., Li, G.Z., Qin, P.F., 2015. Seepage features of high-velocity non-Darcy flow in highly productive reservoirs. J. Nat. Gas Sci. Eng. 27, 1732—1738. https://doi.org/ 10.1016/j.ingse.2015.10.039.
- You, L.X., Liu, H.T., 2002. A two-phase flow and transport model for the cathode of PEM fuel cells. Int. J. Heat Mass Tran. 45 (11), 2277–2287. https://doi.org/ 10.1016/S0017-9310(01)00322-2.
- Yu, D.Z., Mei, R.W., Luo, L.S., et al., 2003. Viscous flow computations with the method of lattice Boltzmann equation. Prog. Aero. Sci. 39 (5), 329–367. https:// doi.org/10.1016/S0376-0421(03)00003-4.
- Zeng, Z.W., Grigg, R., 2006. A criterion for non-Darcy flow in porous media. Transport Porous Media 63 (1), 57–69. https://doi.org/10.1007/s11242-005-2720-3.
- Zhan, H.B., Wen, Z., Gao, G.Y., 2009. An analytical solution of two-dimensional reactive solute transport in an aquifer-aquitard system. Water Resour. Res. 45 (10), W10501. https://doi.org/10.1029/2008wr007479.
- Zhang, M.Y., Lai, Y.M., Li, D.Q., et al., 2013. Experimental study on ventilation characteristics of a concrete-sphere layer and a crushed-rock layer. Int. J. Heat Mass Tran. 59, 407–413. https://doi.org/10.1016/j.ijiheatmasstransfer.2012.12.013.
- Zolotukhin, A.B., Gayubov, A.T., 2021. Semi-analytical approach to modeling forchheimer flow in porous media at meso- and macroscales. Transport Porous Media 136 (3), 715–741. https://doi.org/10.1007/s11242-020-01528-4.